*Presented at the 35th European PV Solar Energy Conference and Exhibition, 24-28 September 2018, Brussels, Belgium*

# CHALLENGES FOR THE QUANTIFICATION OF METAL INDUCED RECOMBINATION LOSSES

D. Herrmann*, S. Lohmüller (née Werner), H. Höffler, A. Fell, A. A. Brand, A. Wolf
Fraunhofer Institute for Solar Energy Systems ISE, Heidenhofstraße 2, 79110 Freiburg, Germany
* Corresponding author: David Herrmann | Phone: +49 (0)761 4588 5049 | E-mail: david.herrmann@ise.fraunhofer.de

ABSTRACT: One major loss mechanism for the currently highly relevant passivated emitter and rear cells (PERC) is locally enhanced recombination at the interface between semiconductor and front side metallization. For investigating these losses in detail, a reliable detection technique is crucial. A method we call calibrated photoluminescence imaging (PLI) method is a promising technique to extract the local dark saturation current density in the metallized area $j_{0,loc}$. To investigate the sources of error of this method, metallized test samples are processed and the influence of sample specific parameters is considered in detail. Additionally, the difference in the resulting $j_{0,loc}$ between the calibrated PLI method and a simulative approach using numerical PLI simulations (Quokka3) is evaluated. We find that the results from the calibrated PLI method strongly depend on the accurate knowledge of the base resistivity $\rho_B$ (including the impact of thermal donors) and less strongly on the reflectivity $R$ of the illuminated side of the sample. In addition, metastable defects in the Si bulk can falsify the results, due to changes in the PLI intensity as a function of the illumination time. The difference in the resulting $j_{0,loc}$ between the calibrated PLI method and the simulative approach is within the error tolerances, which implies that the calibrated PLI method delivers accurate results despite the assumption of a uniform $\Delta n$ throughout the sample. Here, it is important to mention that the non-uniformity of $\Delta n$ is expected to be stronger for structures without a highly doped region at the investigated side (e.g. PERC rear contacts).
Keywords: Photoluminescence, Recombination, Metallization, Quokka3

## 1 INTRODUCTION

During the last years passivated emitter and rear cells (PERC) have gained more and more relevance for both, research institutes and industry [1]. Various authors identified recombination losses induced in the emitter region—especially at the front side metal contacts—to be currently one of the dominating loss mechanisms [2–5]. Although the fraction of metallized surface on the front side of a typical PERC solar cell is just a few percent, the share of recombination losses induced in this area is comparable with the losses in the passivated emitter area. Quantifying the recombination losses at the metal contacts in terms of the local dark saturation current density $j_{0,loc}$ is essential for development of advanced emitters, metallization pastes as well as accurate device simulation. Hence, a reliable and accurate technique to extract $j_{0,loc}$ is needed. A method we call from now on calibrated photoluminescence imaging (PLI) [6, 7] is a method which is frequently used for quantifying $j_{0,loc}$ and which is of rising interest in the PV community. Using this approach the average detected PLI signal (Counts/Pixel*s) is calibrated to an implied open circuit voltage i$V_{oc}$ measured by quasi steady state photoconductance (QSSPC). Thereby the PLI signal can be translated into an i$V_{oc}$ and further with the one-diode equation into a total dark saturation current density $j_0$. Comparing the resulting $j_0$ values of metallized and non-metallized samples $j_{0,loc}$ can be determined with the known metallization area fraction.

However, using this technique, several uncertainties strongly affect the final result. In the present work, the influence of sample parameters such as base resistivity $\rho_B$, metal impurities in the wafer bulk and surface reflectivity $R$ are discussed in detail. Furthermore, the results using the calibrated PLI method are compared to the results using an approach which uses numerical PLI simulations to replicate PLI measurements as described in [8, 9].

## 2 SAMPLE PREPARATION

To investigate the influence of sample specific parameters on the determination of metal induced recombination losses, two samples types, which from now on are called both-sided emitter- and PERC-samples are fabricated, as shown in Fig. 1 a) and b).
Fig. 1 c) exemplary shows the process flow for the fabrication of both-sided emitter-samples. The characterization steps are highlighted in white letters. Sample preparation starts with pseudo-square n-type Czochralski-grown silicon (Cz-Si) wafers with an edge length of 156 mm and a base resistivity of $\rho_B \approx 4\ \Omega$cm determined after thermal donor anneal [10]. After alkaline texturing, a $POCl_3$-based diffusion process in an industrial tube furnace forms phosphorus-doped regions symmetrically on both sides with a sheet resistance of $R_{sh} \approx 130\ \Omega/\square$. Subsequently, the phosphosilicate glass (PSG) layer, which forms during the diffusion process, is removed in hydrofluoric acid (PSG etching). A wetchemical clean is performed, followed by an annealing step in $N_2$ [11] and subsequent deposition of a silicon nitride ($SiN_x$) anti-reflection coating (ARC) on both sides of the both-sided emitter-samples using plasma enhanced chemical vapor deposition (PECVD). Thereafter, a fast firing step is carried out in an industrial conveyor belt furnace to activate the passivation layers. Spatially resolved PLI measurements, using the Modulum tool at the Fraunhofer ISE, and QSSPC measurements, using a Sinton WCT-120 lifetime tester [12], follow. After screen printing a finger grid with 150 fingers of about 40 µm width on one side of the samples using a commercially available silver paste, and contact firing similar to the first fast firing step, an additional PLI measurement is performed using the procedure as described in section 3. PLI measurements on non-metallized reference samples, conducted after a first and a second firing step, confirm that the sample properties in the non-metallized areas are hardly affected by a second firing process. Additionally PERC-samples from *p*-type Cz-Si industrial precursors with an edge length of

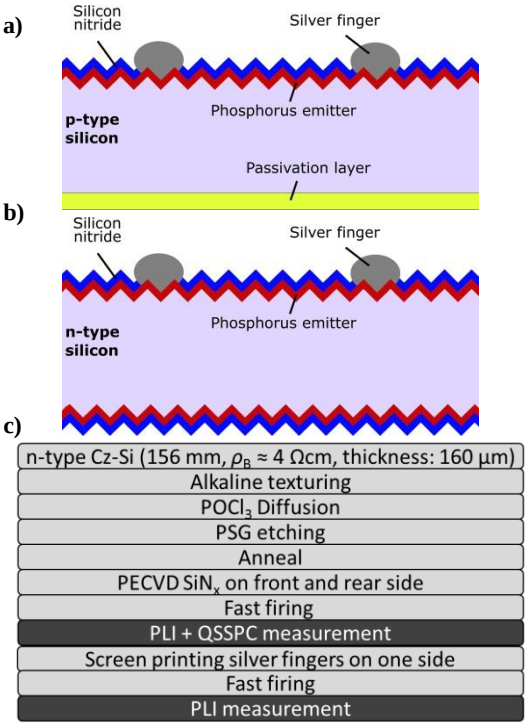


Fig. 1: a) Schematic draw of the PERC-samples and b) the both-sided emitter samples. c) Process flow for the fabrication of both-sided emitter-samples fabricated from n-type Czochralski-grown silicon (Cz-Si) wafers.

156 mm and a nominal resistivity of 1 Ωcm $\leq \rho_B \leq$ 3 Ωcm are fabricated following a similar process route, with the ARC just on the front side.

For the comparison between the calibrated PLI method and the simulative approach, laser ablated samples are used. The samples are fabricated similar to the process flow shown in Fig. 1 and were already investigated in Ref. [13]. Instead of screen printing and the second fast firing step the passivation is locally ablated on one side of the sample via irradiation with a pulsed laser using a pulse duration of 15 ps and a wavelength of 355 nm. A similar ablation process is used for Ni-Cu plated metallizations [14] and is known to cause amorphization of the remaining silicon surface [15], thus inducing high surface recombination velocities, comparable to that of a screen printed metallization. The ablation geometry consists of parallel lines with an ablation width of $w \approx 16$ µm and eight different line distances $d$ from $d = 100$ µm up to $d = 1500$ covering the entire sample area. Also reference samples are processed, for which no laser process is applied.

## 3 APPROACH

This section describes the approach for the determination of the local dark saturation current density used in this work.

A scheme of the measurement steps of the calibrated photoluminescence method is given in Fig. 2. The routine is shown exemplarily for *p*-type PERC-samples fabricated, as described in section 2. Starting from the upper left in the non-metallized state the samples are measured by QSSPC and PLI. The PLI measurement is performed with the passivated rear side pointing upwards to the illumination source and detector. Additionally, two short pass filters with cut-off wavelengths $\lambda_{cutoff,1} = 1050$ nm and $\lambda_{cutoff,2} = 1000$ nm are used to minimize the impact of optical variations of the non-illuminated surface. The averaged PLI-intensity $\bar{\varphi}_1$ in the area where the QSSPC measurement is performed, is linked to the implied open circuit voltage $iV_{OC}$ determined by QSSPC, via the calibration constant $C = \bar{\varphi}_1 / \exp(\frac{iV_{OC}}{V_t})$ as derived in [16], where $V_t$ is the thermal voltage at 25°C. In this step it is essential, that the $iV_{OC}$ is determined at the identical generation rate $G$, at which the PLI measurement is performed, to ensure that the measurement values are determined under preferably similar conditions (similar excess carrier density $\Delta n$).

Using the sample specific $C$, the averaged PLI intensity $\bar{\varphi}$ can be related to an averaged implied open circuit voltage $i\bar{V}_{OC}$ in the non-metallized as well as in the metallized state. Assuming an ideal diode behavior $j_{rec} = j_0 \cdot \exp(iV_{OC}/V_t)$—the subtrahend -1 is neglected, since it is insignificant—, where $j_{rec}$ is the recombination current density, the total dark saturation current density $j_0$ can be extracted with knowledge of $j_{rec}$. During a PLI measurement the samples are in steady state open circuit conditions, leading to equality of recombination current density and generation current density: $j_{gen} = j_{rec}$. The generation current density can be expressed as $j_{gen} = q \cdot (1 - R) \cdot j_\gamma$ where $q$ is the elementary charge, $R$ is the reflectivity of the illuminated sample side and $j_\gamma$ is the photon flux of the illuminating laser on the sample per square centimeter.

Transmission losses can be neglected due to the short absorption length at the applied wavelength $\lambda = 790$ nm, compared to the wafer thickness. Thus, we can determine the total dark saturation current densities of the non-metallized samples $j_{0,non\text{-}metall.}$ as well as the ones of the metallized samples $j_{0,metall.}$ using $C$ and the averaged PLI intensity in the same region of interest (ROI) for the non-metallized ($\bar{\varphi}_2$) and metallized PLI measurement ($\bar{\varphi}_3$). The difference in total dark saturation current density

$$\Delta j_0 = j_{0,metall.} - j_{0,non\text{-}metall.} = j_{rec} \cdot C \cdot (1/\bar{\varphi}_3 - 1/\bar{\varphi}_2) \qquad (1)$$

can be associated to the dark saturation current density in the metallized area $j_{0,loc}$ by

$$\begin{aligned} j_0 &= j_{0,b} + (1 - F) \cdot j_{0e} + F \cdot j_{0,loc} \\ &= j_{0,b} + j_{0,e} + F \cdot (j_{0,loc} - j_{0e}) \qquad (2) \\ \Rightarrow \Delta j_0 &= F \cdot (j_{0,loc} - j_{0,e}), \end{aligned}$$

where $j_{0,b}$ represents the dark saturation current density of the bulk and rear side and $F$ is the metallization fraction of the metallized side. If $j_0$ is now plotted against $F$, $j_{0,loc}$ can be calculated from the slope of the graph $m = j_{0,loc} - j_{0e}$, if $j_{0e}$ is known.

A further approach to quantify the locally enhanced recombination in a certain region is a comparison between numerical PLI simulations using Quokka3 [17] and PLI measurements, as similar proposed in Ref. [8, 9]. Further information about the detailed approach will be published [18]. The major benefit of this simulative approach in contrast to the calibrated PLI is the fact, that it accounts for a lateral and vertical non-homogeneous carrier injection density $\Delta n$ in the sample. The assumption of homogeneous $\Delta n$ is less fulfilled especially for high $j_{0,loc}$ values. Therefore, in this work

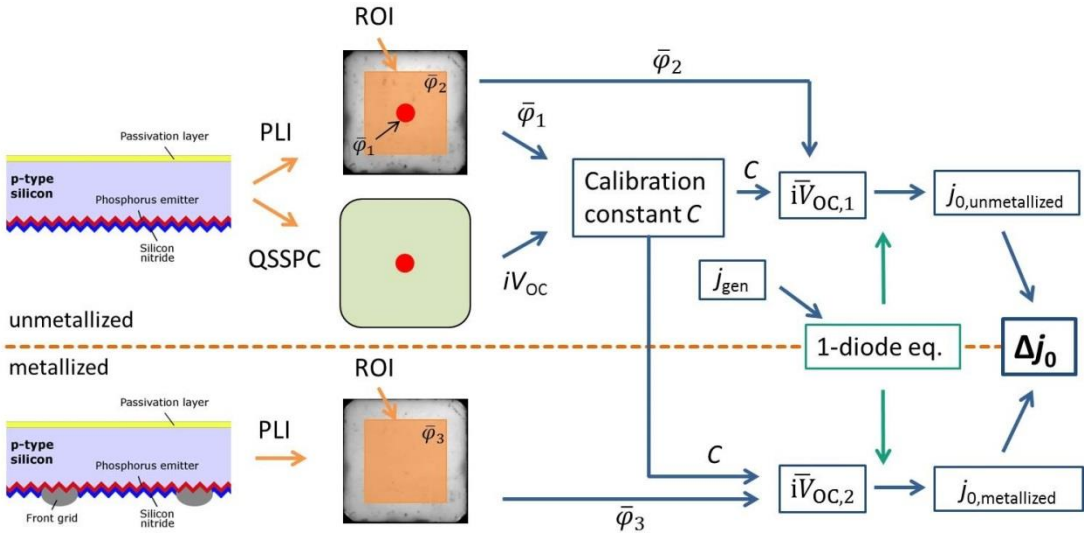


Fig. 2: Scheme of the measurement routine for the calibrated photoluminescence imaging (PLI) method exemplarily shown for *p*-type PERC-samples. Combining the resulting $\Delta j_0$ and the metallization fraction F, $j_{0,loc}$ can be determined. A detailed description of the single steps can be found in section 3.

we use this approach to estimate the influence due to a non-uniform $\Delta n$ on the apparent $j_{0,loc}$ determined by calibrated PLI.

## 4 RESULTS

In this section the influence of sample-specific parameters as $\rho_B$, $R$ and metastable defects in the wafer bulk on the calibrated PLI method are discussed in detail. At first the influence of $\rho_B$ is discussed, which is shown in Fig. 3. On top, the influence of the input parameter $\rho_B$ on the apparent $iV_{OC}$ (left axis) measured by QSSPC in the non-metallized state (at $G_{QSSPC} = G_{PLI}$) and on the apparent $\Delta j_0$ between metallized an non-metallized samples (right axis) using calibrated PLI (see Fig. 2, assuming a rear side reflectivity of $R_{average} = 28\%$) is exemplarily shown for a *p*-type PERC-sample with $\rho_B \approx 1.85\ \Omega$cm (measured after thermal donor annihilation). The $iV_{OC}$ measured by QSSPC is given by

$$iV_{OC} = kT/q \cdot \ln(((\Delta n + N_D)\cdot \Delta n)/n_i^2), \qquad (3)$$

where $k$ is the Boltzmann constant, $T = 25°C$ is the temperature at standard testing conditions, $\Delta n$ is the minority excess carrier density, $n_i$ is the intrinsic charge carrier density(here $n_i = 8.6\cdot10^9\ cm^{-3}$ as it is used in the Sinton Software Version 4.6.0) and $N_D$ is the dopant concentration, which is defined by $\rho_B$.

The wafers are specified with $1\ \Omega cm \le \rho_B \le 3\ \Omega cm$. A variation from $\rho_B = 1\ \Omega$cm to $\rho_B = 3\ \Omega$cm affects the apparent $iV_{OC}$ by more than 25 mV. As explained in section 3, $iV_{OC}$ affects the calibration constant $C$ exponentially and hence the extracted $\Delta j_0$ rises exponentially as a function of $iV_{OC}$. Therefore, the apparent $\Delta j_0$ changes from $\Delta j_0 \approx 70\ fA/cm^2$ to $\Delta j_0 \approx 200\ fA/cm^2$ if $\rho_B$ is changed from $\rho_B = 1\ \Omega$cm to $\rho_B = 3\ \Omega$cm, respectively.

Usually, Cz-Si wafers contain thermal donors, making a representative measurement of $\rho_B$ impossible without an additional thermal donor annihilation process [10] or the etch back subsequently to the process chain. At the bottom of Fig. 3 exemplary measurements of $\rho_B$

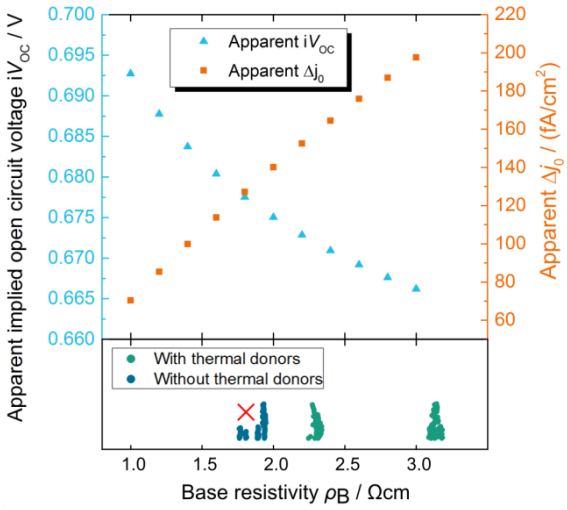


Fig. 3: Influence of the base resistivity $\rho_B$ on the apparent $iV_{OC}$ measured by QSSPC as well as on the apparent $\Delta j_0$ determined by the calibrated PLI method. $\rho_B$ is varied from $\rho_B = 1\ \Omega$cm to $\rho_B = 3\ \Omega$cm similar to the manufacturer specifications of the samples. At the bottom the measured $\rho_B$ values of the *p*-type PERC-samples are given before and after thermal donor annihilation. The base resistivity of the investigated sample is marked with a red cross.

with and without thermal donors are shown, using industrial *p*-type Cz-Si precursors from the same box as used for the experiment of this work. The base resistivity $\rho_B$ decreases by up to more than 1 Ωcm after thermal donor annihilation.

For the measurements shown in Fig. 3, the $\Delta j_0$ results taking into account the values for $\rho_B$ without thermal donors differ by up to approximately 75% compared to the $\Delta j_0$ results using $\rho_B$ measured before diffusion—with thermal donors. In consideration of the strong deviation of the $\Delta j_0$ results an accurate knowledge of $\rho_B$ is crucial for a precise analysis of the metal induced recombination.

A further parameter, which influences the evaluation, is the density of metal impurities within the Si wafer. Fig.

4 shows the normalized averaged PLI intensity as a function of the illumination time at an illumination photon flux of $2.5 \cdot 10^{17}$ cm$^{-2}$s$^{-1}$ (corresponding to 1 sun intensity, which is equivalent to 1000 W/m$^2$) preliminary to the measurement, exemplarily for a *n*-type and a *p*-type sample as described in section 2. The measurement was performed by repetitively illuminating the sample for $t_{ill} = 4$ s and then taking a PLI image with an exposure time of 1 s. The PLI intensity $\varphi$ of the *p*-type sample increases to its maximum within the first 20 s of illumination. The initial $\varphi$ of the exemplarily shown sample is $\varphi \approx 82$ %. This effect can be attributed to iron impurities which form iron-boron pairs (FeB) in the dark. During illumination of the sample, FeB dissociates into interstitial iron ($Fe_i$) and boron (B) [19]. For open circuit conditions with injection carrier densities $\Delta n > 10^{14}$ cm$^{-3}$ the Shockley-Read-Hall (SRH) lifetime of interstitial iron $\tau_{Fei}$ is larger than the respective SRH lifetime of FeB $\tau_{FeB}$ [19]. Therefore, the effective lifetime increases after illumination (Verified by effective lifetime measurements using QSSPC). In contrast the PLI intensity for n-type samples stays constant and is independent on the time of previous illumination, since there are no FeB pairs present.

Using the calibrated PLI method it is important to perform the PLI measurements at a stable state of the samples, at which further illumination does not change the effective lifetime $\tau_{eff}$. Otherwise the measurements before and after metallization are difficult to compare, especially if different exposure times are applied. Therefore, we suggest a measurement procedure—if a similar characteristic as for the *p*-type samples is present—where the samples are illuminated at least 20 s by the PLI laser preliminary to the measurement. Additionally, it has to be mentioned that the strong carrier injection dependency (due to FeB impurities) of the effective lifetime affects the validity of the one-diode equation.

The last sample-specific parameter discussed here, is the reflectivity $R$ of the rear side illuminated during the PLI measurement. On the top of Fig. 5 the influence of $R$ on the apparent implied open circuit voltage $iV_{OC}$ (determined by QSSPC, assuming a fixed optical constant $f_{Abs}$, since the QSSPC measurement was performed with the textured front side pointing upwards, $R$ was found to be almost constant for the front side from sample to sample) and on the apparent $\Delta j_0$ using calibrated PLI is exemplarily shown for one *p*-type sample. By increasing the reflectivity from $R = 0\%$ to $R = 40\%$ the apparent $iV_{OC}$

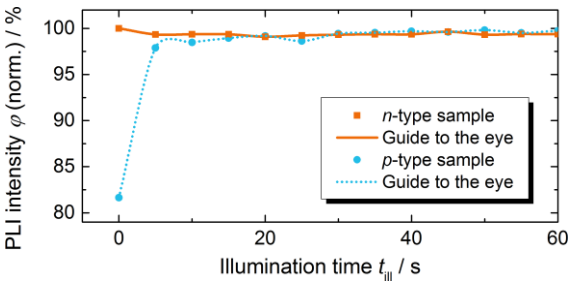


Fig. 4: The normalized PLI intensity $\varphi$ in a certain region of interest as a function of the illumination time $t_{ill}$—at1 sun intensity—preliminary to the measurement is shown for an exemplary *p*-type and n-type sample. The samples are preliminary illuminated by the laser of the PLI setup.

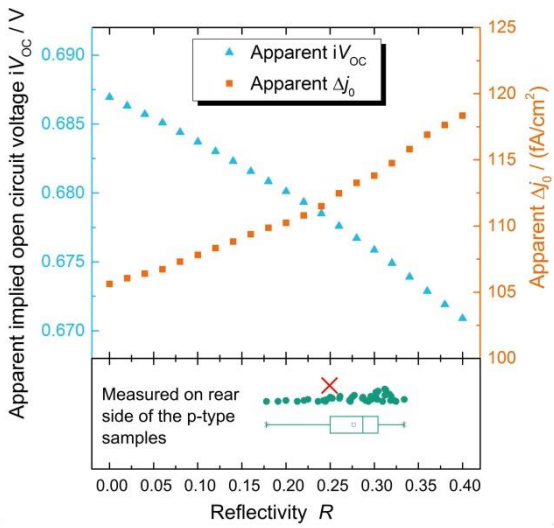


Fig. 5: On top the impact of the rear side reflectivity $R$ on the apparent $iV_{OC}$ as well as the apparent $\Delta j_0$, determined by the calibrated PLI method, is shown. The PLI measurement is performed with the rear side pointing upwards to the illumination source and detector. At the bottom the measured $R$ values of the used set of *p*-type PERC-samples are demonstrated (one measurement per wafer in the wafer center). The $R$ of the investigated sample is marked with a red cross.

drops from $iV_{OC} \approx 687$ mV to $iV_{OC} \approx 670$ mV and the apparent $\Delta j_0$ increases from $\Delta j_0 \approx 105$ fA/cm² to $\Delta j_0 \approx 120$ fA/cm². Two impacts have to be considered. On the one hand $R$ affects the generation rate $G = j_\gamma \cdot (1\text{-}R)/W$, where $W$ is the thickness of the sample. Increasing $R$ leads to a decrease in $G$, since less photons enter the sample. As explained in section 3, the $iV_{OC}$ measured by QSSPC is evaluated at $G$ of the PLI measurement. Therefore, an overestimation of $R$ leads to an underestimation of $iV_{OC}$ and thus, to an overestimation of both, the calibration constant $C$ and $\Delta j_0$ (see section 3). On the other hand, $R$ affects the calculation of the recombination current density $j_{rec} = q \cdot (1\text{-}R) \cdot j_\gamma$ which is linearly connected to $\Delta j_0$ (see section 3). In this case an overestimation of $R$ leads to an underestimation of $j_{rec}$ and thus, to an underestimation of $\Delta j_0$. In our case, the latter aspect is weaker compared to the first, thus these two impacts do not fully compensate each other.

At the bottom of Fig. 5, the measured reflectivity $R$ of the plain passivated rear side of the *p*-type samples (wafer center, one measurement per sample) at the wavelength of the PLI laser $\lambda_{Laser} = 790$ nm is shown. For the used set of identically processed wafers, the results vary within $18\% < R < 33\%$ resulting in a mean value $R_{mean} = (28 \pm 4)\%$. Although our samples show a quite large sample-to-sample variation in $R$ the use of a wrong $R$-value for a specific sample would lead to an error in $\Delta j_0$ of about 5% in the worst case. Therefore the influence of $R$ on the resulting $\Delta j_0$ is less significant than the influence of $\rho_B$.

In Reference [13], the locally enhanced recombination of the laser ablated samples is determined using the calibrated PLI method. The reported value in this publication is $j_{0,loc} = (3700 \pm 500)$ fA/cm$^2$. In our work the identical samples are investigated using the simulative method as described in section 3. The result using this approach is $j_{0,loc} = (4100 \pm 100)$ fA/cm$^2$. Further details of

this evaluation will be published in Ref. [18]. It has to be mentioned that the error estimated for the calibrated PLI approach $\sigma_1 = 500$ fA/cm$^2$ includes also systematical errors, whereas the error for the simulative approach $\sigma_2 = 100$ fA/cm$^2$ only includes the standard deviations of the results from laser ablated samples with different area fractions. The results are in good agreement within the error tolerances.

Theoretically, it is expected that the calibrated PLI underestimates the resulting $j_{0,\mathrm{loc}}$. The underestimation of $j_{0,\mathrm{loc}}$ originates from the assumption of a uniform $\Delta n$. Especially, for high $j_{0,\mathrm{loc}}$ values or high metallization fractions, this condition is violated, as it is also discussed in [20]. Therefore $\Delta n$ is overestimated at the highly recombinative surface and hereby $j_{0,\mathrm{loc}}$ is underestimated. In our comparison we identify a similar tendency.

The results further imply that the 'easy-to-perform' approach of the calibrated PLI delivers results in good accordance with the simulations, even the investigated $j_{0,\mathrm{loc}} > 4000$fA/cm$^2$ induces stronger $\Delta n$ variations than most of the screen printed pastes, which normally induce $j_{0,\mathrm{loc}} \leq 3000$fA/cm$^2$ [21]. For lower $j_{0,\mathrm{loc}}$ values the deviation of $\Delta n$ is expected to be smaller. Additionally, it is important to mention that the results in this work are generated on symmetrical samples with both-sided emitter. For structures without highly doped regions (e.g. PERC rear contacts) the $\Delta n$ deviations are expected to be stronger and therefore the results for $j_{0,\mathrm{loc}}$ between the simulative method and calibrated PLI are expected to differ more significantly.

## 5 SUMMARY

In summary, we find a strong sensitivity of the calibrated PLI method on specific sample parameters. Especially the base resistivity $\rho_\mathrm{B}$ and metastable impurities can falsify the results significantly. For our samples a determination without considering thermal donors can falsify the result by approximately 75%. Excluding the effect of metastable impurities is important, since the measurements before and after metallization should be performed in a similar and stable state. Therefore, an accurate knowledge of the samples' parameters and properties is crucial.

Additionally, a comparison between the simulative approach using Quokka3 and the calibrated PLI method indicates just a minor difference within the error tolerances. We conclude that the results using calibrated PLI with accurate knowledge of the samples' parameters and proper realization delivers accurate results on a full area emitter.

## ACKNOWLEDGEMENT

The authors would like to thank Sebastian Meier-Meybrunn and Jonas Huyeng for the support with the simulations. Further, David Herrmann would like to thank the "Deutsche Bundesstiftung Umwelt DBU" for funding his dissertation project. This work was supported by the German Federal Ministry for Economic Affairs and Energy BMWi and by the industry partners within the research POLDI under contract No. 0324079D. The authors are responsible for the content.

## 5 REFERENCES

[1] ITRPV, "International Technology Roadmap for Photovoltaic: 2016 Results," Jun. 2017. [Online] Available: http://www.itrpv.net/Reports/Downloads/.

[2] P. Saint-Cast *et al.*, "Analysis of the losses of industrial-type PERC solar cells," *Phys. Status Solidi A*, vol. 214, no. 3, p. 1600708, 2017.

[3] M. Müller *et al.*, "Loss analysis of 22% efficient industrial PERC solar cells," *Energy Procedia*, vol. 124, pp. 131–137, 2017.

[4] S. Wasmer, A. A. Brand, J. M. Greulich, "Metamodelling of numerical device simulations to rapidly create efficiency optimization roadmaps of monocrystalline silicon PERC cells," *Energy Procedia*, vol. 214C, 2017.

[5] H. Hannebauer, T. Dullweber, U. Baumann, T. Falcon, and R. Brendel, "21.2%-efficient fineline-printed PERC solar cell with 5 busbar front grid," *Phys. Status Solidi RRL*, vol. 8, no. 8, pp. 675–679, 2014.

[6] S. Herlufsen et al., "Photoconductance-calibrated photoluminescence lifetime imaging of crystalline silicon," *Phys. Status Solidi RRL*, vol. 2, no. 6, pp. 245–247, 2008.

[7] B. Hallam et al., "Photoluminescence imaging for determining the spatially resolved implied open circuit voltage of silicon solar cells," *Journal of Applied Physics*, vol. 115, no. 4, p. 44901, 2014.

[8] M. Ernst, A. Fell, E. Franklin, and K. J. Weber, "Characterization of Recombination Properties and Contact Resistivity of Laser-Processed Localized Contacts From Doped Silicon Nanoparticle Ink and Spin-On Dopants," *IEEE J. Photovoltaics*, vol. 7, no. 2, pp. 471–478, 2017.

[9] A. Fell, D. Walter, S. Kluska, E. Franklin, and K. Weber, "Determination of Injection Dependent Recombination Properties of Locally Processed Surface Regions," *Energy Procedia*, vol. 38, pp. 22–31, 2013.

[10] W. Götz et al., "Thermal donor formation and annihilation at temperatures above 500 °C in Czochralski-grown Si," *Journal of Applied Physics*, vol. 84, no. 7, pp. 3561–3568, 1998.

[11] S. Werner *et al.*, "Key aspects for fabrication of p-type Cz-Si PERC solar cells exceeding 22% conversion efficiency," in *33rd EU PVSEC*, Amsterdam, The Netherlands, 2017.

[12] R. A. Sinton and A. Cuevas, "Contactless determination of current–voltage characteristics and minority-carrier lifetimes in semiconductors from quasi-steady-state photoconductance data," *Appl. Phys. Lett.*, vol. 69, no. 17, pp. 2510–2512, 1996.

[13] H. Höffler et al., "Uncertainty in the Determination of Local Saturation Current Densities," Otsu, Japan, Nov. 14 2017.

[14] A. Grohe *et al.*, "Novel low temperature front side metallisation scheme using selective laser ablation of anti reflection coatings and electroless nickel plating," in *21st EU PVSEC*, Dresden, 2006, pp. 750–753.

[15] J. Bonse, K.-W. Brzezinka, and A.J. Meixner, "Modifying single-crystalline silicon by femtosecond laser pulses: An analysis by micro Raman spectroscopy, scanning laser microscopy and atomic force microscopy," *Applied Surface Science*, vol. 221, no. 1-4, pp. 215–230, 2004.

[16] P. Wurfel, "The chemical potential of radiation," *J. Phys. C: Solid State Phys.*, vol. 15, no. 18, pp. 3967–3985, 1982.

[17] A. Fell, J. Schön, M. C. Schubert, and S. W. Glunz, "The concept of skins for silicon solar cell modeling," *Sol. Energy Mater. Sol. Cells*, vol. 173, pp. 128–133, 2017.

[18] D. Herrmann et al., "to be published,"

[19] D. Macdonald, A. Cuevas, and J. Wong-Leung, "Capture cross sections of the acceptor level of iron–boron pairs in p-type silicon by injection-level dependent lifetime measurements," *J. Appl. Phys.*, vol. 89, no. 12, p. 7932, 2001.

[20] R. Dumbrell, M. K. Juhl, T. Trupke, and Z. Hameiri, "Extracting Metal Contact Recombination Parameters From Effective Lifetime Data," *IEEE J. Photovoltaics*, pp. 1–8, 2018.

[21] T. Fellmeth *et al.*, "Recombination at metal-emitter interfaces of front contact technologies for highly efficient silicon solar cells," *Energy Procedia*, vol. 8, pp. 115–121, 2011.